Journal on Electronic and Automation Engineering

Vol: 4(1), March 2025

REST Publisher; ISSN: 2583-6951 (Online)

Website: https://restpublisher.com/journals/jeae/

DOI: https://doi.org/10.46632/jeae/4/1/9

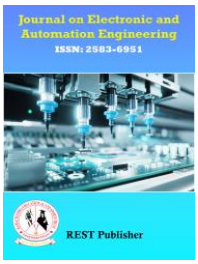

Multipurpose Power Electronic Interface for Plug-In Electric Vehicles with Dual Charging Sources and ANFIS Control

***Sadhu Renuka, P. Haritha, Kadumuru Sree Lekha**

Annamacharya Institute of Technology & Sciences (Autonomous) Kadapa, Andhra Pradesh, India

**Corresponding Author Email: sadhurenukareddy@gmail.com*

Abstract: *This paper presents a multipurpose power electronic interface (PEI) for plug-in electric vehicles (EVs), capable of utilizing dual sources—solar photovoltaic (SPV) and the electrical grid—during the battery charging process. The proposed PEI eliminates the need for additional components or switches to switch between sources or to perform Maximum Power Point Tracking (MPPT), making it a highly efficient solution. The converter, based on a conventional isolated Secondary-ended Primary Inductance Converter (SEPIC), is designed to operate in all vehicular modes: charging, propulsion, and regenerative braking (RB). In charging modes, the converter functions as an isolated SEPIC, providing safe and effective battery charging from both SPV and grid sources. During propulsion and regenerative braking, it operates as a flyback converter while maintaining electrical isolation in all modes for improved safety. The proposed PEI enhances the compactness and functionality of the onboard charger by integrating all modes into a single converter system, making it an ideal solution for electric vehicle applications. The system is controlled by an Adaptive Neuro-Fuzzy Inference System (ANFIS) controller, ensuring optimal performance under varying conditions.*

1. INTRODUCTION

The increasing adoption of plug-in electric vehicles (EVs) has spurred significant advancements in power electronic interfaces (PEIs) for efficient energy management. The need for flexible and reliable solutions to support dual energy sources, such as solar photovoltaic (SPV) systems and the electrical grid, is crucial for improving the sustainability and operational efficiency of EVs. Traditional PEIs often require complex circuitry with additional components or switches for seamless transition between different power sources, introducing both complexity and inefficiency into the charging process. Furthermore, most of these systems fail to address the need for efficient operation in multiple vehicular modes, such as charging, propulsion, and regenerative braking (RB).

To overcome these challenges, this paper proposes a novel multipurpose PEI that seamlessly integrates SPV and grid charging capabilities into a single converter system. Based on an isolated Secondary-ended Primary Inductance Converter (SEPIC), the proposed design eliminates the need for additional switches or components to facilitate maximum power point tracking (MPPT) or switching between power sources. The system operates efficiently in all vehicle modes—charging, propulsion, and regenerative braking—while maintaining electrical isolation for enhanced safety. During charging, the converter functions as an isolated SEPIC to ensure effective and safe battery charging. In propulsion and regenerative braking modes, the converter operates as a flyback converter, ensuring the system remains compact, versatile, and efficient. In addition to its functional design, the proposed PEI is controlled by an Adaptive Neuro-Fuzzy Inference System (ANFIS), which optimizes performance under dynamic operating conditions. The integration of a single converter for all modes simplifies the onboard charging system and enhances the overall performance and safety of EVs, making it a promising solution for future electric vehicle applications.

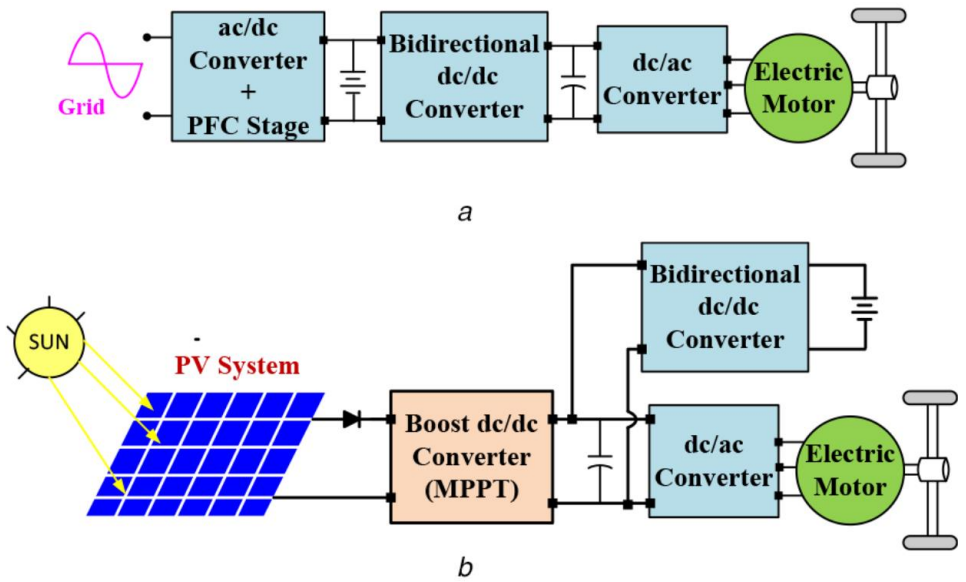

FIGURE 1. Block diagram of chargers (a) Conventional single-stage plug-in charger, (b) Conventional SPV system for a battery charger

As the demand for efficient and reliable power management systems in electric vehicles (EVs) continues to grow, significant progress has been made in the development of on-board chargers (OBCs). Conventional single-stage chargers typically require at least three converters for battery charging and discharging, leading to increased complexity, size, weight, and cost. To address these issues, researchers have proposed integrated chargers that utilize fewer components while maintaining or improving the performance of the charging process. These integrated chargers aim to reduce the number of components needed in comparison to traditional single-stage chargers, thereby improving system efficiency and reducing the overall size and weight of the charger. Integrated chargers can be broadly classified into two types. In the first type, a bidirectional dc/dc converter is placed between the battery and the dc link and is integrated into the charging circuit. In the second type, the electric motor winding and traction converter are used in the charging circuit, often with relays and mechanical switches, thereby eliminating the need for additional inductors in the charging system. The inductor, being the heaviest component in a converter, significantly contributes to the weight of the system. By eliminating or minimizing its use, the overall weight of the charger can be reduced, offering significant advantages in terms of vehicle performance and energy efficiency. However, many of these integrated chargers operate in boost mode, which requires a bidirectional dc/dc converter between the dc link and the battery to provide adequate voltage and current for charging. This additional converter increases the weight and cost of the system. Moreover, there are several challenges and limitations in the existing integrated chargers: (i) the need for specially designed windings, (ii) applicability limited to certain types of electric machines, (iii) difficulty in accessing the neutral point of windings, (iv) reduced reliability due to mechanical contacts, (v) complexity in control and the requirement for extra hardware, and (vi) a tendency to operate in boost mode only, restricting the versatility of the charger. Despite these drawbacks, integrated converters help minimize the size, weight, and cost of the chargers, making them an attractive option for onboard charging systems.

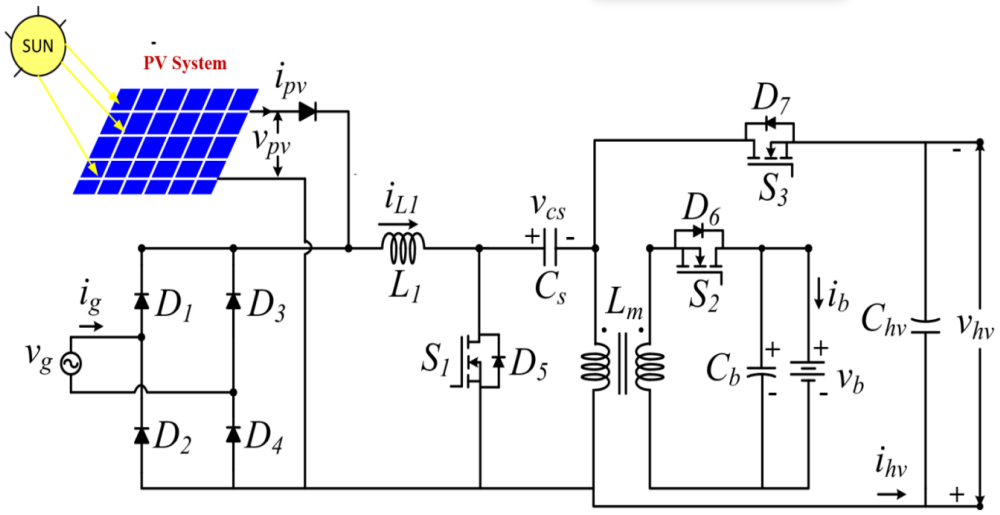

FIGURE 2. Structure of proposed power electronics interface (PEI)

Furthermore, most integrated chargers rely on non-isolated converters to achieve all modes of vehicular operation. Galvanic isolation, often avoided in OBC designs due to its impact on cost, weight, and size, is crucial for ensuring safety in the charger circuit and prolonging the battery life. While galvanic isolation is desirable for safety and reliability, it adds complexity to the design. Moreover, many integrated chargers use either grid power or regenerative braking (RB) for battery charging, but few designs incorporate supplementary renewable energy sources like solar photovoltaic (SPV) systems into the charger architecture. In light of the limitations of current integrated chargers, this paper proposes a novel grid and SPV-based integrated charger with galvanic isolation for all vehicular modes. The proposed charger, as shown in Fig. 2, is based on a conventional isolated secondary-ended primary inductance converter (SEPIC). This converter operates as a SEPIC during battery charging from both the grid and SPV sources, and as a flyback converter during propulsion and regenerative braking modes, offering a versatile solution to power conversion for EVs. The main advantages of the proposed charger over existing integrated chargers include: (a) the provision of galvanic isolation in all vehicle operating modes, ensuring enhanced safety for both the battery and vehicle users, (b) seamless charging from both grid and SPV sources using a single converter, eliminating the need for additional converters or MPPT controllers, (c) reduced reliance on fossil fuel-based electricity by utilizing solar power, and (d) improved reliability with dual sources for battery charging. Additionally, the proposed converter incorporates buck/boost operation in all modes, which is essential for vehicle applications. This feature enables the system to handle a wide range of battery voltages and allows the battery to be charged with a universal input voltage range of 90–260 V. As the battery voltage fluctuates significantly depending on its state-of-charge (SOC), the ability to perform both buck and boost operations ensures flexibility in charging conditions, making the proposed integrated charger a highly effective solution for modern electric vehicles.

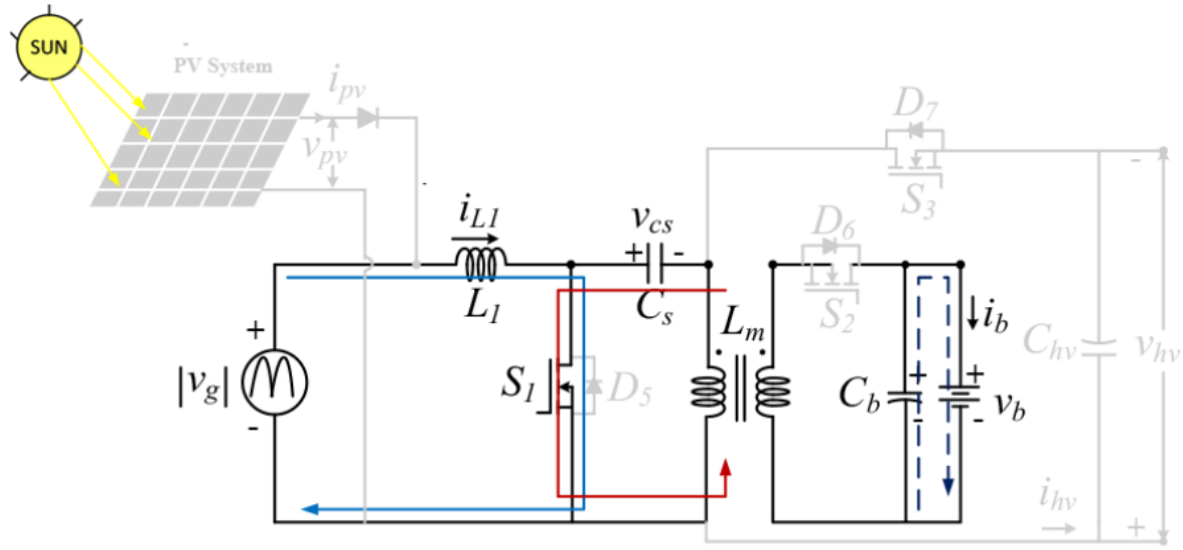

(a)

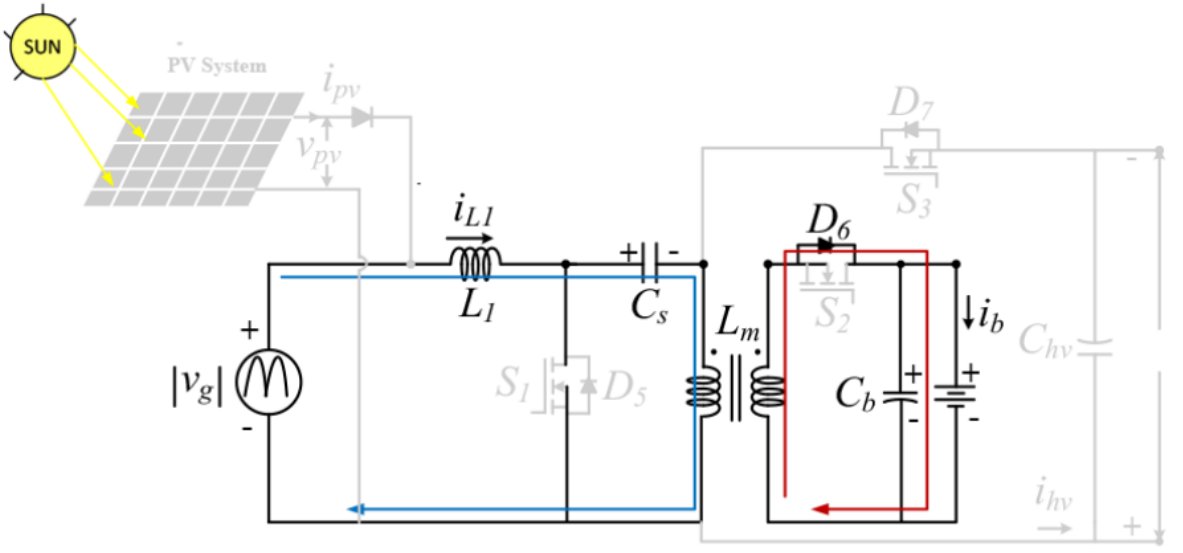

(b)

FIGURE 3. Operation of the converter during PIC mode (a) Switch S1 is ON, (b) Switch S1 is OFF

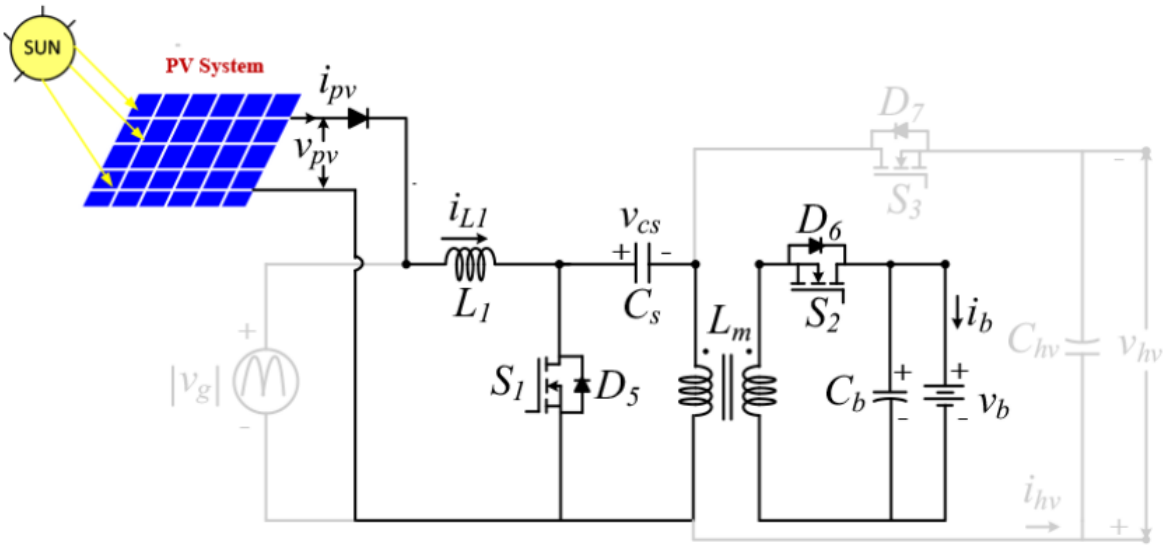

FIGURE 4. Circuit representation for solar battery charging

Operation of the converter in SEPIC and flyback modes is discussed in the following sections. Moreover, operating states of switches and body diodes are given in Table 1.

TABLE 1.States of semiconductor devices in each mode

Mode of operation	Figure	S_1	S_2	S_3	D_5	D_6	D_7
PIC and solar charging	Figs. 3*a* and 4	PWM	OFF	OFF	OFF	OFF	OFF
	Figs. 3*b* and 4	OFF	OFF	OFF	OFF	ON	OFF
PP	Fig. 5*a*	OFF	PWM	OFF	OFF	OFF	ON
RB	Fig. 5*b*	OFF	OFF	PWM	OFF	ON	OFF

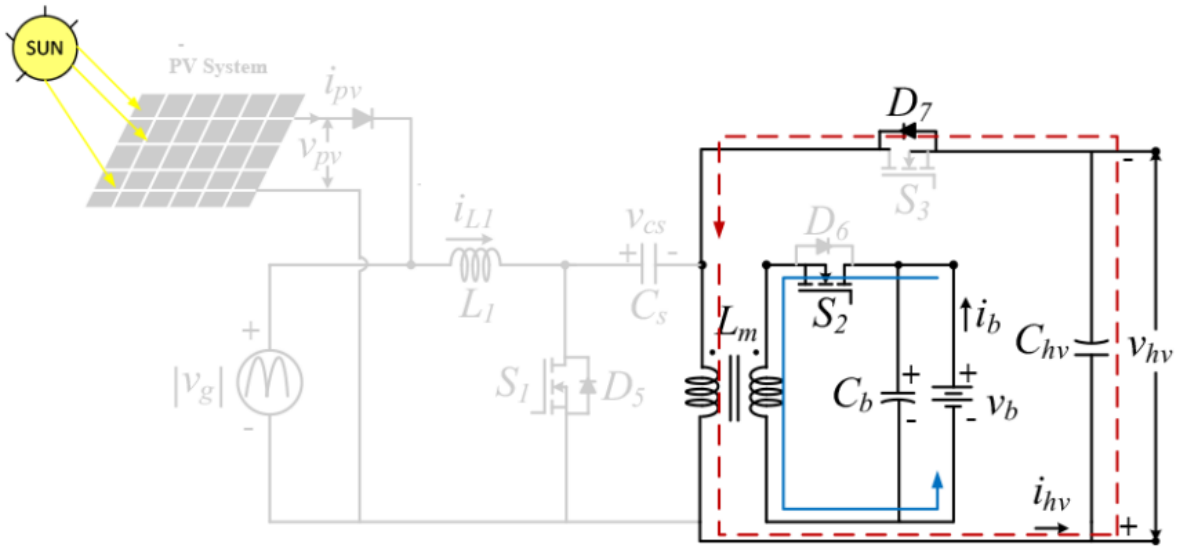

(a)

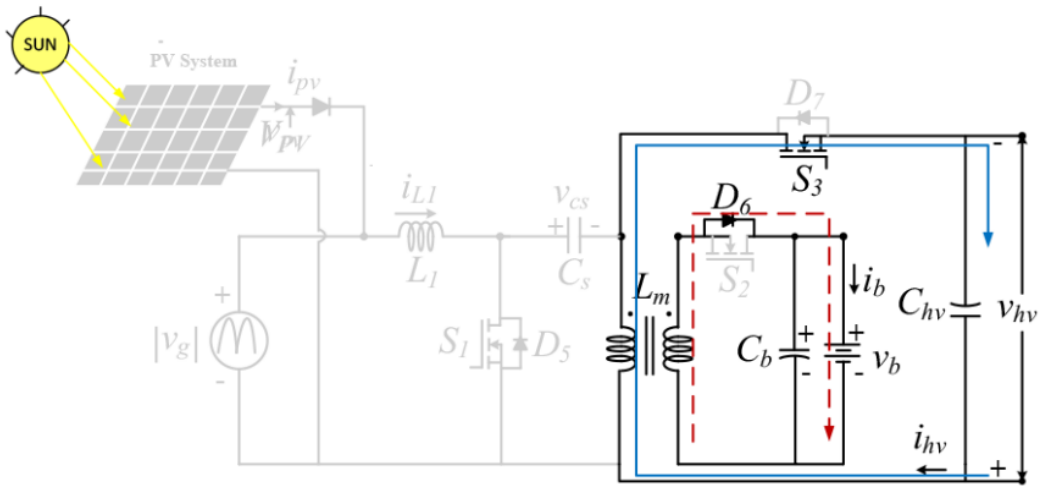

(b)

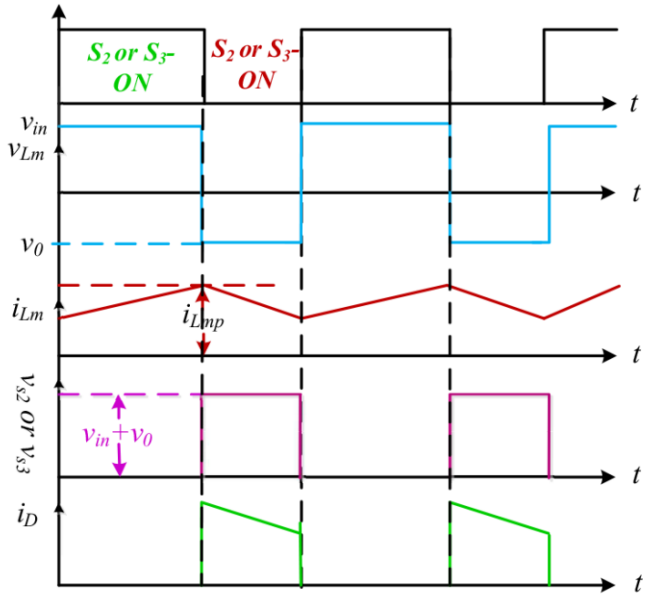

(c)

FIGURE 5. Operation of the converter in (a) PP mode, (b) RB mode and, (c) Operation waveforms of PP and RB modes

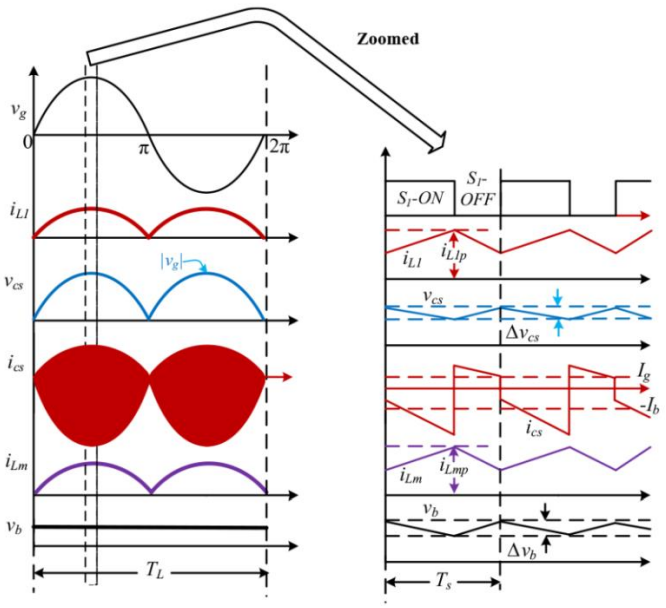

FIGURE 6. Operation waveforms during line and switching cycles

2. SEPIC MODE OF OPERATION

In SEPIC mode of operation, the battery is charged through both the grid and the SPV system. When the battery is charged through the grid, this operation mode is referred to as Plug-in Charging (PIC). PIC Mode: In this mode, the SPV system is deactivated, and the battery is charged from the grid. When switch S1 is turned ON, the current through inductor L1 follows the path indicated by the blue line in Fig. 3a. The electrostatic energy stored in capacitor Cs is converted into magnetic energy and stored in the magnetizing inductance (Lm) of the high-frequency transformer (HFT) through the path indicated by the red line. Meanwhile, capacitor Cb, connected at the battery terminal, supplies energy to the battery. When S1 turns OFF, the stored magnetic energy of Lm is transferred to the battery output as shown by the red lines in Fig. 3b. Additionally, during this mode, the capacitor Chv is charged up to the peak grid voltage through the body diode D7 of switch S3. After this charging process, D7 remains OFF throughout the rest of this mode. The operation waveforms during the line and switching cycles in this mode are shown in Fig. 6. SPV Mode: In this mode, the grid is deactivated, and the battery is charged entirely through the SPV system. The output from the solar panels is fed into the isolated SEPIC converter, where Maximum Power Point Tracking (MPPT) is performed using the SEPIC. The operation of the converter in this mode follows the same sequence as described in the PIC mode. The equivalent circuit for this mode is shown in Fig. 4, and the operation is nearly identical to the PIC mode, except the input source is now the SPV system.

Flyback Operation: During the Propulsion (PP) and Regenerative Braking (RB) modes, the proposed converter operates as a conventional flyback converter. In the following sections, the operation of both modes is discussed with the relevant waveforms as shown in Fig. 5c. In Fig. 5c, vin and v0 represent the input and output voltages of the PP and RB modes, respectively. The current through diode D7 is labelediD in PP mode and through diode D6 in RB mode. Additionally, the current through the magnetizing inductance Lm is shown as iLm in both PP and RB modes.

PP Mode: In PP mode, when switch S2 turns ON, the magnetizing inductance Lm of the high-frequency transformer (HFT) stores energy, and current through Lm is indicated by the solid blue line in Figure a. When S2 turns OFF, the stored energy in inductor Lm is transferred to the DC-link capacitor Chv through the path shown by the red dotted line in Figure a.

RB Mode: The operation during regenerative braking (RB mode), as shown in Fig. 5b, is nearly identical to the PP mode, except it occurs in the reverse direction. In this mode, switch S3 turns ON, and inductor Lm stores energy, with the current flow through Lm represented by the solid blue line. When S3 turns OFF, the stored energy in Lm is transferred to the battery, thus increasing the battery's state-of-charge (SOC).

$$V_b = \frac{d_1(t)}{(1-d_1(t))}\left|v_g(t)\right|$$

where d1(t) is the instantaneous duty ratio and $\left|v_g(t)\right| = V_{gmax}\left|\sin(\omega t)\right|$ hence, the duty ratio d1(t) is obtained as

$$d_1(t) = \frac{V_b}{V_b + \left|v_g(t)\right|} = \frac{V_b}{V_b + V_{gmax}\left|\sin(\omega t)\right|}$$

The value of inductor L1 for allowable ripple current (η) is given as [23]

$$L_1 = \frac{v_g(t)d_1(t)}{\eta i_g(t) f_s} = \left(\frac{V_g^2}{P_g}\right)\frac{d(t)}{\eta f_s}$$

$$= \frac{1}{\eta f_s}\left(\frac{V_g^2}{P_g}\right)\frac{v_b}{V_b + \left|v_g(t)\right|}$$

The maximum inductor ripple current is obtained at the rated conditions, i.e. Vb = Vbmax and input power Pg = Pgmax for a minimum value of input voltage (Vgmin). The input inductor L1 is designed to the peak value of minimum supply voltage 2Vgmin . Using (3), the value of L1 is calculated as 2.82 mH for permitted current ripple 50% of input current (ig) and selected as 3 mH for continuous conduction mode (CCM) of operation.

Design of capacitor Cs

The value of the capacitor Cs is determined for allowable ripple voltage of k% of vcs is given as [22]

$$C_s = \frac{V_b d_1(t)}{k v_{cs}(t) f_s R_L}$$

where vcs is the voltage across capacitor Cs by substituting the expression of vcs(t) = vg(t) , equivalent load resistance, RL = Vb 2 /Pb , and d1(t) in (4), by rearranging we can get

$$C_s = \frac{V_b}{k\left|(v_g(t))\right| f_s \frac{V_b^2}{P_b}}\left(\frac{V_b}{\left|v_g(t)\right| + V_b}\right)$$

$$= \frac{P_b}{k f_s \left|(v_g(t))\right| (v_g(t) + V_b)}$$

The capacitor Cs is calculated at maximum value ripple voltage corresponding to the maximum supply voltage (Vgmax) and at nominal battery voltage (Vb). Now, allowable ripple voltage is 5% of vcs, the value of the capacitor Cs is calculated as 0.724 μF and selected as 1 μF.

3.3 Design of magnetising inductance Lm

The value of magnetising inductance Lm of a high-frequency transformer (HFT) for allowable ripple current ξ % of the input current (ig) is expressed as [24]

$$L_m = V_b \frac{(1 - d_1(t))}{\Delta I_{Lm}(t) f_s} = \frac{V_g^2}{P_g} \frac{1}{\xi f_s} \frac{V_b}{v_g(t) + V_b}$$

where ΔILm(t) = ξ% of the input current and turn ratio of HFT is taken as unity in this case. Therefore, the value of magnetising inductance Lm for a permitted ripple current ξ of 50% is calculated using (6) as 3.06 mH and selected as 3 mH.

Design of capacitor Cb

The capacitor Cb is selected based on second harmonic (100 Hz) voltage ripple. Then the value of the capacitor Cb is given by at low frequency (100 Hz) as [22]

$$C_b = \frac{I_b}{2\omega \Delta V_b} = \frac{((P_b)/(V_b))}{2\omega \delta V_b} = \frac{P_b}{2\omega \delta V_b^2}$$

where δ is the tolerable ripple voltage in the capacitor Cb, ω = 4π f L and f L is the grid frequency (50 Hz). For permitted rippled 3% (δ), the value of the capacitor Cb is calculated using (7) as 1061μF and selected as 1200μF.

Loss Analysis: In this section, the losses associated with both semiconductor and passive components are analyzed for each mode of operation. Since both solar charging and Plug-in Charging (PIC) utilize the SEPIC part of the proposed Power Electronic Interface (PEI), the loss analysis of PIC mode suffices to represent the loss characteristics during solar charging. Loss calculations for PIC, Propulsion (PP), and Regenerative Braking (RB) modes are performed using RMS and average current expressions, as shown in Table 3. The governing equations for loss calculation in each mode can be found in [9].

In Table 2, Pb, Ppp, and PRB represent the power losses for PIC, PP, and RB modes, respectively. From the data presented in Table 2, the total losses (from semiconductor and passive components) in PIC mode range between 4.2% and 7.4%, which is higher compared to the losses observed in PP and RB modes. This increased loss in PIC mode is primarily due to significantly higher passive component losses when compared to those in the PP and RB modes. In PIC mode, the contribution of passive component losses accounts for approximately 57% to 70% of the total losses, while in PP mode, passive component losses contribute between 58% and 63% of the total losses.

The peak efficiency of PIC mode, for grid voltages of 120 V and 240 V, is 95.69% and 93%, respectively. For PP mode, with load powers of 5 kW and 10 kW, the peak efficiency is around 96.2% and 95.8%, respectively. The higher efficiency observed in PP mode is particularly beneficial for vehicle applications, as it results in a greater driving range per charge. This high efficiency makes the proposed converter an excellent choice for next-generation Plug-in Electric Vehicles (PEVs).

Component Lifetime Reliability Analysis:

The lifetime of semiconductor devices typically exceeds that of capacitors and batteries in power electronic systems. In the proposed converter, the high-voltage DC-link capacitor (Chv) is not utilized during PIC mode, while the capacitor

connected to the battery terminals is used during the vehicular modes (SPV charging, PP, and RB). As a result, the proposed converter faces no additional risk of capacitor failure compared to conventional On-Board Chargers (OBCs) [9].
The switch S2, or its body diode (D6), conducts in all modes, meaning it experiences regular cycling, which may slightly reduce its lifetime. The failure of S2 could impact all vehicular modes, leading to a marginal decrease in the overall reliability of the proposed converter when compared to traditional OBCs.
Switch S1 conducts during PIC and SPV charging, while switch S3, or its body diode (D7), is active during PP and RB modes. Typically, PP mode in vehicle applications involves higher power ratings compared to other modes. Consequently, S1 is less likely to fail compared to S3, as the frequency of cycling for S3 is higher during high-power operations. However, if S1 fails, it would not affect PP and RB modes, as these modes would still function with S3.
In conclusion, while the lifetime reliability of the converter is slightly lower than that of conventional OBCs due to the increased cycling of S2 and S3, the overall impact on system reliability is manageable. The modular nature of the converter also ensures that failure in one switch does not lead to a total system failure, maintaining operational flexibility in the vehicle.

Comparative analysis:
The proposed converter is compared with reported integrated chargers in terms of the total number of components, buck/boost operation, solar charging and galvanic isolation. A detailed comparative analysis has been shown in Table 4.

TABLE 2. Total losses of the converter in ac/dc and dc stages with Vb = 300 and Vhv = 400 V

P_b, kW	P_{pp}, kW	P_{RB}, kW	V_g	Total semiconductors losses, P_S, W			Total passive components losses, P_p, W		
				PIC (ac/dc stage)	PP (dc/dc stage)	RB (dc/dc stage)	PIC (ac/dc stage)	PP (dc/dc stage)	RB (dc/dc stage)
1.8	2	0.5	120	34.68	16.81	10.1	46.29	22	11.2
3.2	5	0.8	240	55.63	197.81	14.1	81	117	16.1
6.6	10	1	240	147.1	62.18	16.2	343	212	17.1

TABLE 3. Current stresses on semiconductor devices and passive components

Devices	PIC		PP		RB	
	RMS	Average	RMS	Average	RMS	Average
S_1	$I_{gRMS}\sqrt{1+\alpha\frac{8}{3\pi}}$	$I_{gRMS}\frac{2\sqrt{2}}{\pi}$	NC		NC	
S_2, xfmr secondary	NC		$\sqrt{I_b^2 d_2 + \frac{d_2^3 V_b}{12 f_s^2 L_m^2}}$	$d_2 I_b$	NC	
S_3, xfmr primary	NC		NC		$\sqrt{I_b^2 d_3 + \frac{d_3(1-d_3)^2 V_b^2}{12 f_s^2 L_m^2}}$	$d_3 I_{hv}$
D_6, xfmr secondary	$I_b\sqrt{\frac{3}{2}+\frac{16}{3\pi}\alpha}$	$\frac{I_{gRMS}2\sqrt{2}}{\pi}\alpha$	NC		$\sqrt{I_b^2(1-d_3) + \frac{(1-d_3)^3 V_b^2}{12 f_s^2 L_m^2}}$	$I_b(1-d_3)$
D_7, xfmr primary	NC		$\sqrt{I_b^2(1-d_2) + \frac{d_2(1-d_2)V_b^2}{12 f_s^2 L_m^2}}$	$I_{hv}(1-d_2)$	NC	
C_s, xfmr primary	$I_{gRMS}\sqrt{\alpha\frac{8}{3\pi}}$	0	NC		NC	
L_1	I_{gRMS}	$I_{gRMS}\frac{2\sqrt{2}}{\pi}$	NC		NC	

Where RMS = root mean square, NC = noconducting $\alpha = \frac{N_2}{N_1}\frac{V_{gmax}}{V_b}$, Ihv = average dc-link current, Ib = average battery current, Vb and Vhv = average battery voltage and dc-link voltage, respectively, IgRMS = grid RMS current and xfmr = transformer.

TABLE 4. Comparative analysis of the proposed converter

Charger topologies	Mode of operation				Number of components				Galvanic isolation
	PIC	Solar charging	PP	RB	Switch	Diode	Inductor	Capacitor	
integrated converter [12]	buck/boost	NA	buck/boost	buck/boost	6	9	1	2	no
integrated converter [25]	boost	NA	boost	buck	5	1	1	2	no
integrated converter [21]	boost	NA	buck/boost	buck/boost	4	4	1	2	no
integrated converter [8]	boost	NA	buck/boost	buck/boost	4	4	2	3	no
proposed integrated converter	buck/boost	buck/boost	buck/boost	buck/boost	3	4	2	3	yes

From Table 4, it can be observed that none of the existing integrated chargers incorporate both galvanic isolation and solar charging capabilities. This makes the proposed charger more efficient and reliable compared to the currently reported integrated chargers. The integrated chargers discussed in [12] do feature buck/boost operations in each mode, but they

require a large number of components. As a result, multiple devices are involved in the current path, leading to higher losses and lower efficiency across all modes of operation. In contrast, chargers reported in [8, 21, 25] only implement boost capabilities in PIC mode. This limitation means that the battery cannot be charged when the peak grid voltage exceeds the battery voltage, which can occur when the battery's state of charge (SOC) is high. This leads to a reduced charging effectiveness under certain conditions.
The chargers in [21, 25] have fewer components and lower stresses on the devices during operation, which translates to higher efficiency in each mode compared to the proposed charger. Additionally, charger [8] demonstrates low stresses on the components in each mode and exhibits higher efficiency in the Propulsion (PP) and Regenerative Braking (RB) modes, primarily due to the reduction in conduction losses during these modes.

Control algorithms
The control structure of the proposed PEI for all modes has been shown in Fig.

PIC mode : In PIC mode, a two-loop Proportional-Integral (PI) controller, denoted as Gib(z), is employed to charge the battery. The control system is structured in two loops for improved regulation of the charging process:
1. Outer Loop (Power Controller): The outer loop functions as a power controller, which generates a reference signal that is used by the inner controller. This reference signal is derived based on the desired power output to the battery, ensuring the system provides optimal power for charging.
2. Inner Loop (PI Controller): The inner loop consists of a PI controller (GiL(z)), which adjusts the operation of the converter by regulating the current. The output of the inner controller is compared with a carrier signal to generate the Pulse-Width Modulation (PWM) signal for controlling switch S1.
The PWM signal generated from this comparison controls the operation of switch S1, determining the appropriate switching frequency and duty cycle to ensure efficient battery charging in PIC mode.

SPV mode: Mathematical Analysis of ANFIS-based MPPT Control
In the proposed MPPT system, we integrate the Adaptive Neuro-Fuzzy Inference System (ANFIS) controller for more precise and dynamic tracking of the maximum power point (MPP). The system uses the SEPIC converter for efficiently charging the battery from the solar photovoltaic (SPV) system, ensuring optimal power extraction. To understand the behavior of the system and its performance, we first review the mathematical modeling of the components and controllers involved.
1. Maximum Power Point Tracking (MPPT)
The fundamental equation for determining the power output of a solar panel is given by:

$$P_{PV} = V_{PV} \times I_{PV}$$

where:
- PPV is the power output from the PV panel.
- VPV is the output voltage of the PV panel.
- IPV is the output current of the PV panel.

The goal of the MPPT controller is to operate the solar system at the maximum power point PMPP, where the product of the voltage and current is maximized. The MPPT controller will adjust the duty cycle DDD of the SEPIC converter to achieve this optimal power output.

ANFIS Control for MPPT: In contrast to traditional MPPT algorithms like P&O, the ANFIS-based MPPT control adapts dynamically to varying environmental conditions. The ANFIS controller learns from the system's performance over time, combining fuzzy logic for decision-making and neural networks for learning and optimization.
The ANFIS controller receives two key inputs:
- PV voltageVPV
- PV currentIPV

The goal of the ANFIS controller is to generate an optimal duty cycle D that maximizes the output power PPV. The relationship between the duty cycle and the output power can be derived from the converter's voltage and current control equation:

$$P_{PV} = \frac{V_{dc} \times I_{PV}}{D}$$

where:
- Vdc is the dc-link voltage.
- IPV is the current produced by the PV panel.
- D is the duty cycle that controls the output voltage of the SEPIC converter.

The ANFIS controller uses fuzzy rules and membership functions to model the relationship between the inputs (VPVand IPV) and the output (duty cycle D).

Let the fuzzy inference system (FIS) be defined by the following general form of rules:

IF Input 1 is A and Input 2 is B, THEN Output is C

The membership functions for input variables VPVand IPVare typically Gaussian or triangular functions that fuzzify the input values. The fuzzy inference system then applies the fuzzy rules to derive a crisp output, which in this case is the duty cycle DDD that maximizes the output power.

Mathematically, the process can be represented as follows:

$$D = f(V_{PV}, I_{PV}, \theta)$$

Where:

- fff represents the fuzzy rule-based mapping.
- θ\thetaθ represents the parameters of the membership functions that the ANFIS model optimizes during the training phase.

Training of ANFIS Controller: During the training phase, the **ANFIS** system adjusts its parameters (membership functions) to minimize the error between the predicted and actual power points. This training is done using a **least-squares** optimization method, where the system iteratively adjusts the parameters to fit the real-world data obtained from the solar panel's performance.

The training algorithm typically involves two steps:

- Forward pass: The inputs VPV and IPV are passed through the fuzzy inference system to compute the duty cycle.
- Backward pass: The error is propagated backward, and the parameters of the membership functions are adjusted to minimize the error in the output power.

The training process ensures that the ANFIS controller accurately models the relationship between the PV panel's input parameters and the optimal duty cycle to maximize power extraction.

PP and RB modes: The control block diagram for PP and RB modes has been shown in Fig. 7, which is closed with red dotted lines. In both the modes, the two-loop PI controller is used to give the PWM pulses for switches S2 and S3. Moreover, the inner PI controller is used for both the modes. The control targets of PP mode are to fix the dclink voltage at reference valued for smooth operation of vehicle. The reference dc-link voltage is compared with measured dc-link voltage and error is supplied to the outer PI controller, which generates a reference signal for the inner PI controller. The output of the inner PI controller is compared to a triangular wave and generates PWM pulses for switch S2. In RB mode, usually, the input reference quantity can be torque or speed, which is determined by the driver [21]. The error between the reference and measured quantities is fed to the outer PI controller and generates reference charging power (Pb), which is then divided by instantaneous battery voltage (vb) to generate a reference signal for the inner PI controller. The parameters of each PI controller are set through trial and error based tuning method.

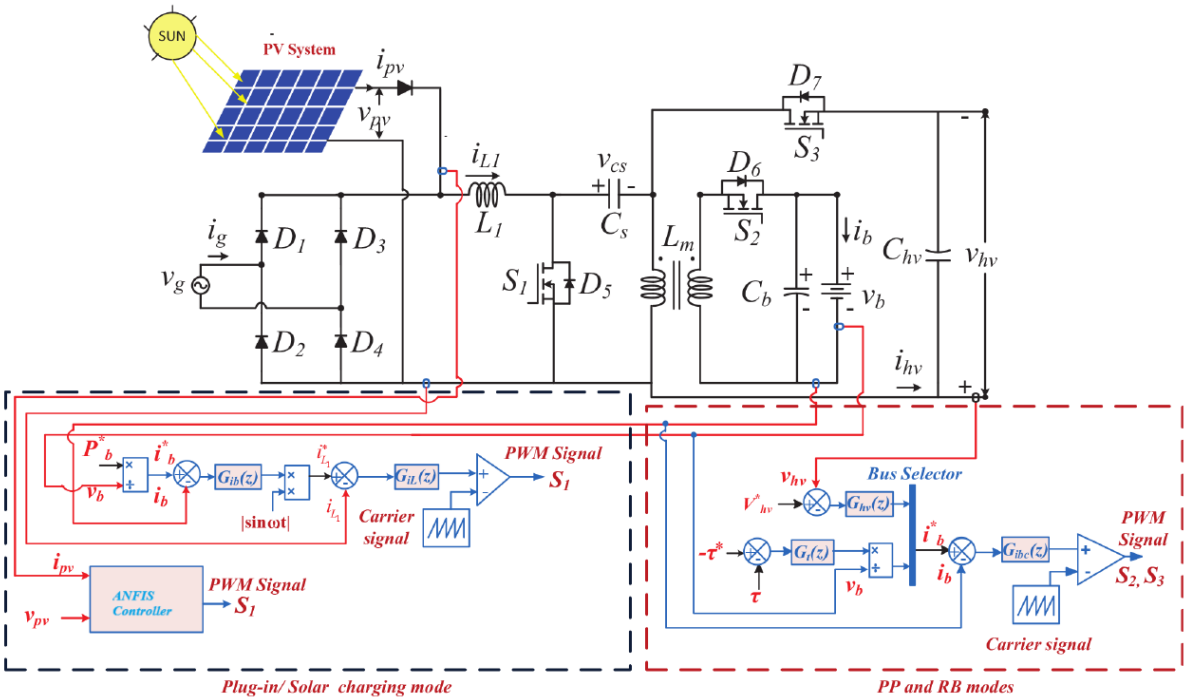

FIGURE 7. Control structure of a proposed system

3. RESULTS AND DISCUSSIONS

Simulation Results of the Proposed Converter with ANFIS-based MPPT Control

The simulation of the proposed converter has been verified in the MATLAB/Simulink environment with the following parameters: grid voltage Vg=220 V, battery nominal voltage Vb=300 V, charging power Pcharging=1.2 kW, and dc-link voltage Vhv=400 V. The simulation results for the PIC mode using an ANFIS-based MPPT controller are shown in Fig. 9.

1. PIC Mode Operation with ANFIS-based MPPT

In PIC mode, the battery is charged through the grid, while the converter operates in a Power Factor Correction (PFC) mode to shape the grid current. The ANFIS-based MPPT controller dynamically adjusts the duty cycle to track the maximum power point of the solar panel, ensuring efficient power extraction. The results are illustrated in the following waveforms:

- Fig. 9a shows the grid voltage and grid current, which are in-phase with a sinusoidal shape, indicating the converter is operating under unity power factor (UPF) condition. The ANFIS controller ensures this operation by adjusting the duty cycle to maintain UPF throughout the charging process.
- Fig. 9b and Fig. 9c show the battery voltage and battery current, respectively, at a 20% state of charge (SOC). The battery current waveform exhibits low-frequency oscillations (100 Hz), a characteristic of single-stage chargers. The maximum peak-to-peak battery current ripple is observed to be twice the average battery current.

While the battery current ripple can be suppressed by adding an inductive filter in series with the battery, the size and cost of this filter depend on the battery type and the overall compactness of the charger. The measured grid RMS current and average battery current at 1.2 kW charging power are 5.8 A and 3.90 A, respectively.

2. Solar Panel Output and MPPT Control

Table 5 presents the parameters of the SPV system, and Fig. 10 illustrates the power vs. voltage curve of the solar panel. The maximum power from the solar panel is obtained at around 800 W at 1000 W/m2 solar irradiation and 400 W at 500 W/m2. The output of the solar panel under MPPT control is shown in Fig. 11. The average output current is approximately 15 A, and the voltage at MPPT operation is 53 V.

The battery charging from the maximum power of the solar panel (800 W) is confirmed by Fig. 12, which shows the battery voltage and current during charging. The measured battery voltage and battery current during solar charging are approximately 309 V and 2.45 A, respectively. The calculated battery power is 757.05 W, resulting in a converter efficiency of 94.6% during solar charging.

3. PP Mode (Driving Operation)

In PP mode, the battery supplies power to the dc-link capacitor to support the vehicle's acceleration. The dc-link voltage is regulated to remain constant at 400 V to ensure smooth operation of the vehicle. Fig. 13 shows the dynamic response of the converter during step load changes:

- At t=1s, the load power increases from 1 kW to 2 kW.
- At t=2s, the load power decreases back to 1 kW.
- At t=3s, the load power again increases to 2 kW.

During these changes, the dc-link voltage remains stable at 400 V, as shown in Fig. 13a. The corresponding changes in battery voltage and battery current are shown in Figs. 13b and 13c, respectively. The measured battery current for 1 kW and 2 kW loads are approximately 3.4 A and 6.9 A, respectively, and the corresponding battery powers are calculated as 1050.6 W and 2132.1 W. The simulation efficiency of the converter at 1 kW and 2 kW loads is 95.2% and 93.8%, respectively.

4. RB Mode (Regenerative Braking)

In RB mode, the battery is charged with the regenerative braking energy from the motor. This mode involves harvesting energy during deceleration and feeding it back into the battery for storage.

4. CONCLUSION

In this paper, a compact multifunctional Power Electronics Interface (PEI) has been proposed for onboard applications in Plug-in Electric Vehicles (PEVs). The proposed PEI operates effectively in all vehicular modes, including grid charging, solar charging, driving operation, and regenerative braking.

Key features and advantages of the proposed system:

- Dual sources for battery charging: The system can charge the battery from both the grid and SPV, reducing reliance on fossil fuels.
- Galvanic isolation in each mode ensures safety and enhances reliability for both the battery and the vehicle.
- Buck/Boost operation across all modes allows the system to handle a wide range of input and output voltages, ensuring compatibility with various charging sources and vehicle requirements.
- The ANFIS-based MPPT controller improves the efficiency of solar charging by dynamically adjusting the duty cycle for optimal power extraction from the solar panel.

The compact design integrates the SPV system through the front-end charging converter, eliminating the need for an additional DC/DC converter for MPPT. The dynamic performance of the proposed converter has been tested in simulation,

demonstrating its effectiveness in handling step load changes in PP mode and battery charging from both the grid and solar energy.In summary, the proposed PEI not only ensures high reliability and efficiency but also contributes to the evolution of electric vehicle (EV) technology, especially in regions where dedicated EV charging stations are not widely available.

REFERENCES

[1]. 'SAE electric vehicle and plug-in hybrid electric vehicle conductive charge coupler'. SAE std. J1772, 2010.

[2]. Patil, D., Sinha, M., Agarwal, V.: 'A cuk converter based bridgeless topology for high power factor fast battery charger for electric vehicle application'. 2012 IEEE Transportation Electrification Conf. and Expo (ITEC), Dearborn, MI, USA, 2012, pp. 1–6

[3]. Shi, L., Meintz, A., Ferdowsi, M.: 'Single-phase bidirectional AC-DC converters for plug-in hybrid electric vehicle applications'. 2008 IEEE Vehicle Power and Propulsion Conf., Harbin, China, 2008, pp. 1–5

[4]. Yilmaz, M., Krein, P.T.: 'Review of battery charger topologies, charging power levels, and infrastructure for plug-in electric and hybrid vehicles', IEEE Trans. Power Electron., 2013, 28, (5), pp. 2151–2169

[5]. Onar, O.C., Kobayashi, J., Erb, D.C., et al.: 'A bidirectional high-powerquality grid interface with a novel bidirectional noninverted buck–boost converter for PHEVs', IEEE Trans. Veh. Technol., 2012, 61, (5), pp. 2018– 2032

[6]. Bendien, J.C., Fregien, G., van Wyk, J.D.: 'High-efficiency on-board battery charger with transformer isolation, sinusoidal input current and maximum power factor', IEE Proc. B - Electr. Power Appl., 1986, 133, (4), pp. 197–204

[7]. Singh, A.K., Pathak, M.K.: 'An improved two-stage non-isolated converter for on-board plug-in hybrid EV battery charger'. 2016 IEEE 1st Int. Conf. on Power Electronics, Intelligent Control and Energy Systems (ICPEICES), New Delhi, India, 2016, pp. 1–6

[8]. Singh, A.K., Pathak, M.K.: 'Single-phase bidirectional ac/dc converter for plug-in electric vehicles with reduced conduction losses', IET Power Electron., 2018, 11, (1), pp. 140–148

[9]. Singh, A.K., Pathak, M.K.: 'Single-stage zeta-sepic-based multifunctional integrated converter for plug-in electric vehicles', IET Electr. Syst. Trans., 2018, 8, (2), pp. 101–111

[10]. Singh, A.K., Pathak, M.K.: 'A multi-functional single-stage power electronic interface for plug-in electric vehicles application', Electr. Power Compon. Syst., 2018, 46, (2), pp. 135–148

